Thermoacoustic Computed Tomography with Large Planar Receivers

(Published in: Inverse Problems 20(5): 1663–1673, 2004)

M. Haltmeier[1] and O. Scherzer[1] and P. Burgholzer[2] and G. Paltauf[3]

[1] Department of Computer Science, Universität Innsbruck,
Technikerstraße 25, A-6020 Innsbruck, Austria.
Markus.Haltmeier@uibk.ac.at, Otmar.Scherzer@uibk.ac.at.
[2] Upper Austrian Research, Hafenstraße 47-51, A-4020 Linz, Austria.
Peter.Burgholzer@uar.at.
[3] Karl-Franzens-Universität Graz, Department of Experimental Physics,
Universitätsplatz 5, A-8010 Graz, Austria.
Guenter.Paltauf@uni-graz.at.

Abstract

Thermoacoustic imaging is a promising new modality for nondestructive evaluation. So far point measurement data for thermoacoustic imaging are used. In this paper we propose a novel measurement setup with relatively large piezo foils (planar receivers) and an according real time imaging algorithm based on the Radon transform. We present numerical simulations for simulated and real world data.

AMS Subject Classification: 92C55, 44A12, 65R10

1 Introduction

Thermoacoustic Computed Tomography (TCT) is a promising new modality for imaging which utilizes *thermoacoustic* (sometimes also called *optoacoustic* or *photoacoustic*) effects [6] of an absorbing medium; when a sample is illuminated by a short electromagnetic pulse, such as visible light, or radio wave, it induces an acoustic wave. The generated pressure field of the acoustic wave depends on the spatially varying absorption density $\psi(x)$ of the sample. In *thermoacoustic imaging* the goal is to recover the density function ψ from measurement data of the acoustic pressure taken outside the illuminated sample (see e.g. [12, 9, 15]).

In the literature, analytical formulas for calculating the density function from measurement data of the pressure have been derived for various sample geometries, such as planes, spheres, cylinders, and circles [4, 15, 16, 17, 9, 10, 8]. In practical experiments these formulas are applicable if measurement data are collected with small receivers around the sample surface. Since small receivers are used to simulate point measurement data, this approximation causes some blurring in the reconstruction with analytical inversion

formulas. In order to handle the blurring Xu and Wang [19] derived analytical expressions of the blurring kernels for various sample surfaces and shapes of receivers.

In contrast to more common approaches outlined above that use inversion of the spherical mean operator we use inversion of the standard Radon transform. The data required for this inversion algorithm can be collected with a relatively *large* planar receiver which is rotated tangentially to a sphere (cylinder) surrounding the sample. Note that in contrast to previous work we do *not* consider the measurement data an approximation of point measurement data and thus we can avoid undesirable blurring. Moreover, the proposed experiment turns out to be extremely robust against noise (cf. section 5).

The outline of this work is as follows: in section 2 we resume the photoacoustic principles. The novel imaging technique is presented in section 3 and section 4. We briefly describe an experimental setup (cf. section 5) for collecting the imaging data used in our inversion technique; a detailed discussion of the experimental setup is intended to be published in a forthcoming article. Finally, in section 6 some numerical experiments for real and synthetic data are presented.

2 Thermoacoustic Tomography

In thermoacoustics, when a sample is illuminated by a pulsed electromagnetic wave, the absorbed power produces heat and results in mechanical expansion of the absorber, which in turn produces a pressure wave.

Let $\hat{I}_{\mathrm{em}}(x,\hat{t})$ denote the *radiation intensity* of the electromagnetic wave and $\psi(x)$ the spatially varying absorption coefficient. Then the *absorbed power* per volume unit is given by

$$\hat{I}_{\mathrm{em}}(x,\hat{t})\psi(x)\ .$$

It can be shown (see e.g. [6, 12, 9, 15]) that the generated *thermoacoustic pressure field* $p(x,t)$ satisfies the inhomogeneous wave equation

$$\left(\frac{1}{v_s^2}\frac{\partial^2}{\partial\hat{t}^2} - \triangle\right) p = \frac{\beta}{c_p}\frac{\partial(\hat{I}_{\mathrm{em}}\psi)}{\partial\hat{t}}\ . \tag{1}$$

Here c_p denotes the *specific heat capacity*, β the *thermal expansion coefficient* at constant pressure, and v_s the *speed of sound*. In our application with pulsed electromagnetic waves we can assume that

$$\hat{I}_{\mathrm{em}}(x,\hat{t}) =: \frac{c_p}{v_s\beta} I(x) j(\hat{t})\ .$$

Here I is the *normalized intensity* and j represents the *temporal shape* of the electromagnetic pulse. In mathematical terms the pulse function $j \in C_0^\infty(\mathbb{R})$

is assumed to have small support $[-\tau, \tau]$ (where $\tau \ll 1$), to be non-negative, and to satisfy

$$\int_{\mathbb{R}} j(\hat{t})\, d\hat{t} = 1 \,, \quad \text{and} \quad \int_{\mathbb{R}} \hat{t} j(\hat{t})\, d\hat{t} = 0 \,. \tag{2}$$

In particular as τ tends to 0, j approximates the δ-distribution. After rescaling by $t = \hat{t} v_s$ the equation for the pressure p (1) reads as follows

$$\left(\frac{\partial^2}{\partial t^2} - \triangle \right) p = I\psi \frac{dj}{dt} \,. \tag{3}$$

The solution of (3) is uniquely determined by specifying appropriate initial conditions. We use

$$p(x, -1) = 0 \,, \quad \text{together with} \quad \frac{\partial p}{\partial t}(x, -1) = 0 \,, \tag{4}$$

to represent the fact that there is no pressure before the experiment starts (at time $\hat{t} = -\tau$).

The solution of (3) and (4) is given by

$$p := j *_t q \,, \tag{5}$$

where $*_t$ is the convolution with respect to t and

$$q(x,t) := \frac{\partial}{\partial t} \left(\frac{t}{4\pi} \int_{S^2} (I\psi)(x + t\sigma)\, d\Omega(\sigma) \right) \,. \tag{6}$$

Here S^2 denotes the two-dimensional unit sphere with surface measure $d\Omega$ (see e.g. [7]). The product of the normalized intensity of the electromagnetic wave and the absorption coefficient

$$f(x) := I(x)\psi(x) \tag{7}$$

is called *energy deposition* function. Note that q satisfies the homogenous wave equation

$$\left(\frac{\partial^2}{\partial t^2} - \triangle \right) q(x,t) = 0 \,, \tag{8}$$

together with inhomogeneous initial conditions

$$q(x, 0) = f(x) \,, \quad \text{and} \quad \frac{\partial q}{\partial t}(x, 0) = 0 \,. \tag{9}$$

Thermoacoustic tomography is concerned with the inverse problem of recovering the energy deposition function f of a sample from temporal measurement data of the thermoacoustic pressure field measured with several detectors outside the sample.

3 A novel reconstruction algorithm based on planar measurement data

The approaches presented in the literature so far rely on point measurement data based on the integral geometric problem of reconstruction a function from its integrals over certain spheres (see e.g. [4, 1, 2, 3, 15]).

In this section we present a novel algorithm for thermoacoustic imaging, where we use the recorded pressure P acting on a planar ultrasound receiver which is rotated tangentially to a sphere S^2 around the sample. In mathematical terms P is the average of the pressure field function p over the receiver. We emphasize that in our inversion technique we only use the function P defined on a three dimensional domain (sphere $\times$ time) and not p (which is a function defined on the four dimensional space $\times$ time domain). In this section we assume that the laser impulse is relatively short, in which case the function j can be considered an approximation of the δ-distribution, and in turn we can identify p and q.

The tangent plane at a point $\sigma \in S^2$ is given by

$$E_\sigma := \left\{ x \in \mathbb{R}^3 : \langle \sigma, x \rangle = 0 \right\} .$$

In our further considerations we make use of the *Radon transform* (for more background on the Radon transform we refer to [13, 5])

$$\mathbf{R} : C_0^\infty(B_1(0)) \to C^\infty(S^2 \times \mathbb{R})$$

defined by

$$(\mathbf{R}f)(\sigma, r) = \int_{E_\sigma} f(r\sigma + y)\, dE_\sigma(y) , \tag{10}$$

and the operator

$$\mathbf{Q} : C_0^\infty(B_1(0)) \to C^\infty(S^2 \times [0, \infty))$$

defined by

$$(\mathbf{Q}f)(\sigma, t) := \int_{E_\sigma} q(\sigma + y, t)\, dE_\sigma(y) , \tag{11}$$

where q is the unique solution of (8) and (9). Note, that in the experimental setup (cf. section 5) the acoustic pressure field $q(x, t)$ itself does not need to be measured but only the averaged data $Q(\sigma, t) = (\mathbf{Q}f)(\sigma, t)$ is required.

In the following we state a fundamental relation between the operators $\mathbf{Q}$ and $\mathbf{R}$ based on a classical commutation relation between the wave operator and the Radon transform.

Theorem 3.1. *Let $f \in C_0^\infty(B_1(0))$. Then*

$$(\mathbf{Q}f)(\sigma, t) = (\mathbf{R}f)(\sigma, 1 - t)/2 , \quad \textit{for all } \sigma \in S^2 , t \geq 0 . \tag{12}$$

Proof. Let q be the unique solution of (8), (9) and denote by

$$Q_\sigma(r,t) := \mathbf{R}(q(\cdot,t))(\sigma,r) := \int_{E_\sigma} q(y + r\sigma, t)\, dE_\sigma(y)$$

the Radon transform of $q(x,t)$ with respect to x. Using a well known commutation relation of the Radon transform with the wave Operator [5] we see that $Q_\sigma(r,t)$ satisfies the one dimensional wave equation

$$\left(\frac{\partial^2}{\partial t^2} - \frac{\partial^2}{\partial r^2}\right) Q_\sigma = 0 \tag{13}$$

for all $\sigma \in S^2$ together with inhomogeneous initial conditions

$$Q_\sigma(r,0) = (\mathbf{R}f)(\sigma,r)\ , \quad \text{and} \quad \frac{\partial Q_\sigma}{\partial t}(r,0) = 0\ . \tag{14}$$

Using D'Alembert's formula the unique solution of (13) and (14) is given by

$$Q_\sigma(r,t) = \frac{1}{2}\Big((\mathbf{R}f)(\sigma,r+t) + (\mathbf{R}f)(\sigma,r-t)\Big)\,. \tag{15}$$

Since f is compactly supported in $B_1(0)$ we see $(\mathbf{R}f)(\sigma,1+t) = 0$ and hence from (15) it follows that $(\mathbf{Q}f)(\sigma,t) = Q_\sigma(1,t) = (\mathbf{R}f)(\sigma,1-t)/2$. □

Theorem 3.1 allows to carry over properties of the Radon transform to the operator $\mathbf{Q}$. To exploit this observation we use the following notation:

$C_0^\infty(S^2 \times \mathbb{R})$ denotes the set of functions $g \in C^\infty(S^2 \times \mathbb{R})$ which are compactly supported in $S^2 \times \mathbb{R}$. Let g be in $C_0^\infty(S^2 \times \mathbb{R})$, then we define

$$(\mathbf{Q}^\dagger g)(x) := -\frac{1}{2\pi^2} \int_{S^2_+} \frac{\partial^2 g}{\partial t^2}\,(\sigma, 1 - \langle x, \sigma\rangle)\ d\Omega(\sigma)\,, \tag{16}$$

where S^2_+ denotes the right half unit sphere, i.e.,

$$S^2_+ := \big\{\sigma = (\sigma^1,\sigma^2,\sigma^3) \in S^2 : \sigma^1 \geq 0\big\}\ . \tag{17}$$

Corollary 3.2. *Let $f \in C_0^\infty(B_1(0))$, then*

$$(\mathbf{Q}f)(\sigma,t) = 0\ , \quad \textit{for all } \sigma \in S^2,\ t \geq 2\ . \tag{18}$$

Moreover, $\mathbf{Q}^\dagger = \mathbf{Q}^{-1}$ on the range of $\mathbf{Q}$.

Proof. From the definition of the Radon transform (10) it follows, that $(\mathbf{R}f)(\sigma,r) = 0$ for $r \notin (-1,1)$. Thus, from (12) it follows that for $t \geq 2$

$$(\mathbf{Q}f)(\sigma,t) = (\mathbf{R}f)(\sigma,1-t)/2 = 0\ .$$

Let g be in the range of $\mathbf{Q}$, i.e., $g = \mathbf{Q}f$. Due to (18) g is in the domain $\mathcal{D}(\mathbf{Q}^\dagger)$ of $\mathbf{Q}^\dagger$. From the inversion formula of the (3-dimensional) Radon transform (cf. [13, p. 20]) it follows that

$$\begin{aligned} f(x) &= -\frac{1}{8\pi^2}\int_{S^2} \frac{\partial^2(\mathbf{R}f)}{\partial t^2}(\sigma, \langle x,\sigma\rangle)\, d\Omega(\sigma) \\ &= -\frac{1}{8\pi^2}\int_{S^2_+\cup S^2_-} \frac{\partial^2(\mathbf{R}f)}{\partial t^2}(\sigma, \langle x,\sigma\rangle)\, d\Omega(\sigma) \\ &= -\frac{1}{8\pi^2}\int_{S^2_+} \left(\frac{\partial^2(\mathbf{R}f)}{\partial t^2}(\sigma, \langle x,\sigma\rangle) + \frac{\partial^2(\mathbf{R}f)}{\partial t^2}(-\sigma, -\langle x,\sigma\rangle)\right) d\Omega(\sigma)\,, \end{aligned}$$

where S^2_- denotes the left half unit sphere. Using that $(\mathbf{R}f)(\sigma, r) = (\mathbf{R}f)(-\sigma, -r)$ we find that

$$f(x) = -\frac{1}{4\pi^2}\int_{S^2_+} \frac{\partial^2(\mathbf{R}f)}{\partial t^2}(\sigma, \langle x,\sigma\rangle)\, d\Omega(\sigma)\,.$$

Then, from (12) it follows that

$$f(x) = -\frac{1}{2\pi^2}\int_{S^2_+} \frac{\partial^2 g}{\partial t^2}(\sigma, 1-\langle x,\sigma\rangle)\, d\Omega(\sigma) = \mathbf{Q}^\dagger g\,.$$

This shows $\mathbf{Q}^\dagger = \mathbf{Q}^{-1}$ on the range of $\mathbf{Q}$. □

From Corollary 3.2 we see that the thermoacoustic inverse problem of recovering the energy deposition function f in (7) from measurement data $\mathbf{Q}f$ on $S^2_+ \times [0,2)$ can be solved uniquely with (16).

Since f is supported in $B_1(0)$ it follows from (6) that $q(\cdot, t)$ is compactly supported in $B_{1+t}(0)$. Thus in the definition of $\mathbf{Q}f$ (cf. (11)) the integration over E_σ can be replaced by integration over the disc $D_\sigma(\sqrt{8})$, where

$$D_\sigma(\rho) := \{y \in E_\sigma : \|y\| < \rho\}\,, \quad (\rho \geq 0)\,. \tag{19}$$

This result is practically relevant since it shows that in experiments the averaged data has to be collected on the *bounded* disc (instead on an *un*bounded plane). The physical explanation for this is that a wave initiated at point x travelling for 2 time units propagates in $B_2(x)$. The intersection of $\bigcup_{x\in B_1(0)} B_2(x)$ with E_σ is the smallest set to collect information of each wave initiated in $B_1(0)$.

The above result also reveals that in order to recover the energy deposition function of an object of diameter d the proposed strategy requires an ultrasound detector which contains a disc of diameter $\sqrt{8}d$ and rotates tangentially to a hemisphere around the object.

4 Deconvolution

Here, in contrast to the previous section, we assume that an approximation of the function j, representing the temporal shape of the electromagnetic pulse, by a δ-distribution is not valid. In this situation the data collected with our measurement setup (cf. section 3) are given by

$$\int_{E_\sigma} (j *_t q)(\sigma + y, t) dE_\sigma(y) = (j *_t \mathbf{Q}f)(\sigma, t) \; .$$

In practical experiments the recorded pressure signal is the function $(j *_t \mathbf{Q}f)$ convolved in time with the impulse response function w of the detector, e.g., a thin piezoelectric film. Thus the actual data available for the inversion process is $w *_t j *_t \mathbf{Q}f(\sigma, t)$ for $(\sigma, t) \in S^2 \times \mathbb{R}$.

In the following we show how the solution of the thermoacoustic inverse problem is affect by the convolution of the data:

Theorem 4.1. *For any $f \in C_0^\infty(B_1(0))$*

$$\mathbf{Q}^\dagger \left(w *_t j *_t \mathbf{Q}f \right) = k * f$$

with

$$k(x) := \begin{cases} -\frac{1}{4\pi\|x\|} \Big((w *_t j)'(\|x\|) - (w *_t j)'(-\|x\|) \Big) \; , & \text{if} \quad x \neq 0 \; , \\ -\frac{1}{2\pi} (w *_t j)''(0) \; , & \text{if} \quad x = 0 \; . \end{cases} \tag{20}$$

Here $(w *_t j)'$ and $(w *_t j)''$ are the first and second time derivatives of $w *_t j$ and $*$ denotes the 3-dimensional convolution operator

$$(k * f)(x) := \int_{\mathbb{R}^3} k(x - y) f(y) \, dy \; .$$

Proof. In the following we make use of the operator $\mathbf{D}$, defined by $(\mathbf{D}\varphi)(t) = \varphi(1 - t)$. The inverse of $\mathbf{D}$ is given by $\mathbf{D}$. For $\varphi \in C_0^\infty(S^2 \times \mathbb{R})$

$$(\mathbf{R}^\sharp \varphi)(x) := \int_{S^2} \varphi \left(\sigma, \langle \sigma, x \rangle \right) \, d\Omega(\sigma)$$

denotes the *backprojection* operator (cf. [13, p. 13]) and hence

$$\mathbf{R}^\dagger \varphi = -\frac{1}{8\pi^2} \, \mathbf{R}^\sharp \varphi'' \; . \tag{21}$$

Then, for g in the range of $\mathbf{R}$ (cf. [13, p. 20]) we have $\mathbf{R}^{-1} g = \mathbf{R}^\dagger g$. From (12) it follows that

$$\mathbf{Q}^\dagger (w *_t j *_t \mathbf{Q}f) = 2 \, \mathbf{R}^\dagger \mathbf{D} \Big((1/2) \, w *_t j *_t (\mathbf{D}\mathbf{R}f) \Big) = \mathbf{R}^\dagger (w *_t j *_t \mathbf{R}f) \; .$$

To prove the assertion we show that

$$\mathbf{R}^\dagger(w *_t j *_t \mathbf{R}f) = k * f.$$

Using (21) and the property of the backprojection operator stated in [13, p. 14] it follows that

$$\mathbf{R}^\sharp(\varphi *_t \mathbf{R}f) = (\mathbf{R}^\sharp\varphi) * f\,, \tag{22}$$

and we find

$$\mathbf{R}^\dagger(w *_t j *_t \mathbf{R}f) = -\frac{1}{8\pi^2}\mathbf{R}^\sharp((w *_t j)'' *_t \mathbf{R}f) = -\frac{1}{8\pi^2}(\mathbf{R}^\sharp(w *_t j)'') * f\,.$$

It remains to prove that

$$(\mathbf{R}^\sharp(w*_t j)'')(x) = \begin{cases} 2\pi/\|x\|\Big((w *_t j)'(\|x\|) - (w *_t j)'(-\|x\|)\Big)\,, & \text{if} \quad x \neq 0\,, \\ 4\pi(w *_t j)''(0)\,, & \text{if} \quad x = 0\,. \end{cases}$$

For $x = 0$ we have

$$(\mathbf{R}^\sharp(w *_t j)'')(x) = \int_{S^2} (w *_t j)''(0)\, d\Omega(\sigma) = 4\pi(w *_t j)''(0)\,.$$

For $x \neq 0$ we choose a positive orientated orthonormal basis y_1, y_2, $x/\|x\|$. The function

$$\begin{aligned} G : (-1,1) \times (0,2\pi) &\to S^2\,, \\ (r,\theta) &\mapsto (r/\|x\|)\, x + \sqrt{1-r^2}\,\Big(\cos(\theta)y_1 + \sin(\theta)y_2\Big) \end{aligned}$$

is injective with *Jacobian* identically one. Therefore, since the range of G differs from S^2 by a set of surface measure zero,

$$\begin{aligned} \int_{S^2} (w *_t j)''(\langle x,\sigma\rangle)\, d\Omega(\sigma) &= \int_{-1}^{1}\int_0^{2\pi} (w *_t j)''(r\|x\|)\, d\theta\, dr \\ &= 2\pi/\|x\|\Big((w *_t j)'(\|x\|) - (w *_t j)'(-\|x\|)\Big)\,. \end{aligned}$$

□

Theorem 4.1 reveals two possibilities to recover the energy deposition function f from the measurement data $w *_t j *_t \mathbf{Q}f$.

1. The first option is to deconvolve (with respect to time) $w *_t j *_t \mathbf{Q}f$ first, and then to recover the energy deposition from $\mathbf{Q}f$.

2. The second option is to use (20) to recover $k * f$ first, and then to deconvolve k and f with respect to the space variable. In many practical applications this deconvolution step can be avoided if the laser impulse is short and the piezoelectric film is sufficiently thin.

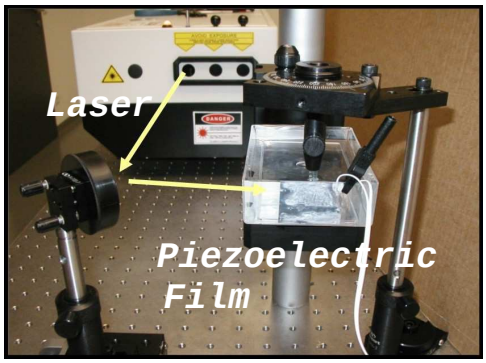

Figure 1: Experimental setup: A cylindrically symmetric object is rotated along the central axis. Every 5° the sample is illuminated by a short laser pulse and the thermoacoustic pressure signal is recorded with a piezoelectric film.

5 Experimental setup

An experimental setup for collecting imaging data for recovering an object with cylindrical symmetry is shown in Figure 1. The experimental setup for collecting imaging data to recover non symmetric objects is intended to be discussed in a forthcoming paper.

In the experiment a cylindrically symmetric object consisting of three cylindrical absorbers with diameters two, three respective four millimeters was mounted on a frame and was rotated around the central axis. The thermoacoustic pressure signal was recorded with a 25 μm (micrometers) thick film of piezoelectric PVDF (Polyvinylidene Fluoride), which generated an electric signal proportional to the total pressure acting on the piezoelectric film. The electric signal was picked up from aluminium coatings on either side of the film, amplified with a charge amplifier and recorded with a digital storage oscilloscope.

Since the thickness of the film is very small compared to the size of the acoustic sources and consequently the impulse response function is short compared to the duration of the acoustic signals, w can very well be approximated by a δ-distribution.

The piezoelectric film was glued on the flat surface of an acrylic glass block. The object with the 3 cylindrical absorbers fitted in a cylinder with a diameter of 10 mm. Therefore the detecting film had to include a disc with a diameter of at least $10\sqrt{8}$ (≈ 28) mm. We took a 50 mm times 40 mm film to be able to have some space between the rotated object and the detector.

Every 5° the sample is illuminated by a short laser pulse of $\hat{t} = 20$ ps (picoseconds). Hence the function j, representing the temporal shape of the

laser pulse, can also be approximated by a δ-distribution.

In this case the thermoacoustic imaging problem reduces to the inversion of the operator $\mathbf{Q}$.

For a cylindrically symmetric object the imaging problem is two-dimensional. In the following we describe the reduction of the three-dimensional reconstruction formula to the case of an object with cylindrical symmetry. Let

$$\bar{f}(x^1, x^2) := \int_{-1}^{1} f(x^1, x^2, x^3)\, dx^3 \tag{23}$$

be the *averaged* energy deposition function along the *central* axis x_3 of the object. In the experiment described above we collect measurement data

$$\bar{g}(\theta(\alpha), t) := (\mathbf{Q}f)(\sigma(\alpha), t) \tag{24}$$

for $\alpha = 0,\ 5^\circ,\ 10^\circ, \ldots, 175^\circ$, where

$$\begin{aligned} \sigma(\alpha) &:= (\theta(\alpha), 0) \in S^1 \times \{0\}\ , \text{ with} \\ \theta(\alpha) &:= (\cos(\alpha), \sin(\alpha)) \in S^1\ . \end{aligned}$$

Note that in this case $E_{\sigma(\alpha)}$ is spanned by the two vectors $y_1 := (\sin(\alpha), -\cos(\alpha), 0)$ and $y_2 := (0, 0, 1)$. For $y \in E_{\sigma(\alpha)}$ we write $y = y^1 \cdot y_1 + y^2 \cdot y_2$.

In the following we provide a reconstruction formula for $\bar{f}$ using the measurement data $\bar{g}$.

Theorem 5.1. *Let $f \in C_0^\infty(B_1(0))$. Then*

$$\bar{f}(x) = \frac{i}{\pi} \int_0^\pi \left(\mathbf{H}\, \frac{\partial \bar{g}}{\partial t} \right) (\theta(\alpha), 1 - \langle x, \theta(\alpha) \rangle) d\alpha\ , \tag{25}$$

where

$$(\mathbf{H}\varphi)(t) := \frac{1}{\pi} \fint_{\mathbb{R}} \frac{\varphi(s)}{t - s}\, ds := \frac{1}{\pi} \lim_{\varepsilon \to 0+} \int_{\mathbb{R} \setminus (-\varepsilon, \varepsilon)} \frac{\varphi(s)}{t - s}\, ds$$

is the Hilbert transform *and $\fint$ denotes the principal value of an integral.*

Proof. From the definitions of $\bar{f}$ and $\bar{g}$, (10) and (12) it follows that

$$\begin{aligned} \bar{g}(\theta(\alpha), t) &= (\mathbf{Q}f)(\sigma(\alpha), t) = (\mathbf{R}f)(\sigma(\alpha), 1 - t)/2 \\ &= \frac{1}{2} \int_{E_{\sigma(\alpha)}} f((1 - t)\sigma(\alpha) + y)\, dE_{\sigma(\alpha)} \\ &= \frac{1}{2} \int_{\mathbb{R}} \bar{f}((1 - t)\theta(\alpha) + y^1 \cdot y_1)\, dy^1 \\ &= (\mathbf{R}_2 \bar{f})(\theta(\alpha), 1 - t)/2\ . \end{aligned}$$

Here $\mathbf{R}_2$ denotes the two-dimensional Radon transform. (25) follows from the inversion formula of the two-dimensional Radon transform (cf. [13, p. 20]). $\square$

6 Numerical inversion

In our numerical simulations we aim to recover $\bar{f}$ (the averaged energy deposition function) from measurement data $\bar{g}$ (24).

There is considerable literature on the inversion of the two-dimensional Radon transform (see e.g. [14]). In our numerical implementation we replace (25) by a stable approximation, the so called filtered backprojection (FBP) algorithm (see [13, p. 102 ff.]), which is outlined below: Let $\{w_\epsilon : \mathbb{R} \to \mathbb{R} : \epsilon > 0\}$ be a family of smooth and even functions. With w_ϵ we associate the function

$$W_\epsilon(x) := (\mathbf{R}_2^\sharp w_\epsilon)(x) = \int_{S^1} w_\epsilon(\langle x, \theta\rangle)\, d\theta = 2\int_0^\pi w_\epsilon(\langle x, \theta(\alpha)\rangle)\, d\alpha\ .$$

$\mathbf{R}_2^\sharp$ denotes the (2-dimensional) *backprojection* operator (see e.g. [13, p. 13]). The functions w_ϵ are chosen in such a way that $W_\epsilon \to \delta$ (delta-distribution) for $\epsilon \to 0$. Hence w_ϵ and W_ϵ satisfy

$$\mathbf{R}_2^\sharp(w_\epsilon *_t \mathbf{R}_2\bar{f}) = W_\epsilon * \bar{f} \to \bar{f} \text{ as } \epsilon \to 0\,, \text{ for all } \bar{f} \in C_0^\infty(B_1(0))\ . \qquad (26)$$

We refer to (22) where we have used this result already in the 3-dimensional setting. From

$$\begin{aligned}
\mathbf{R}_2^\sharp\Big(w_\epsilon *_t \mathbf{R}\bar{f}\Big)(x) &= 2\mathbf{R}_2^\sharp\Big(w_\epsilon *_t (\mathbf{D}\bar{g})\Big)(x) \\
&= 2\mathbf{R}_2^\sharp\mathbf{D}\Big(w_\epsilon *_t \bar{g}\Big)(x) \\
&= 4\int_0^\pi \Big(w_\epsilon *_t \bar{g}\Big)\left(\theta(\alpha), 1 - \langle x, \theta(\alpha)\rangle\right)\, d\alpha\,,
\end{aligned}$$

and (26) it follows that for $x \in \mathbb{R}^2$

$$4\int_0^\pi \Big(w_\epsilon *_t \bar{g}\Big)\left(\theta(\alpha), \langle x, 1 - \theta(\alpha)\rangle\right)\, d\alpha \ \longrightarrow \bar{f}(x) \text{ as } \epsilon \to 0\ .$$

For $\epsilon > 0$ fixed we use $4\int_0^\pi \Big(w_\epsilon *_t \bar{g}\Big)\left(\theta(\alpha), \langle x, 1 - \theta(\alpha)\rangle\right)\, d\alpha$ for imaging of $\bar{f}$ in the following two examples:

1. We have used measurement data (24) collected with the experiment described in section 5 to recover three cylindrical objects. The numerical reconstruction is plotted in Figure 2.

2. The second data set is synthetic data involving a variety of small structures, which is recovered from measurement data $\mathbf{Q}f$ collected at a sampling interval of 0.3°. With this rate even small details can be detected (cf. bottom left Figure 3). The bottom right figure shows a reconstruction where the measurement data Q is synthetically perturbed by 10% additive Gaussian noise. We note that 10% noise in

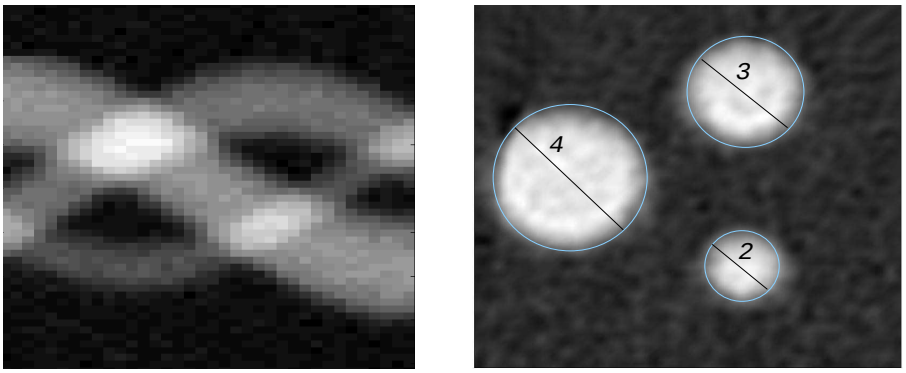

Figure 2: *Top Left:* Measured thermoacoustic pressure signal (time versus angle). *Top Right:* Reconstruction from real measurement data.

the simulated data is practically unrealistic (to high). This work cannot be compared with previous published experiments where isolated point measurement data have been used. Mathematically highly oscillating noise for isolated point measurement data is averaged over a large detector area. In fact in the experiments we did not observe high oscillatory noise at all.

Conclusion

In this paper we have suggested to use large planar detectors to collect thermoacoustic data that can easily be related to the Radon transform of the energy deposition function. This allows to apply standard algorithms for thermoacoustic reconstruction. In practical experiments, the data required for imaging can be collected with relatively large piezo foils. The experimental setup has been presented and numerical reconstructions with real and synthetic data have been given.

Acknowledgement

The work of M.H. and O.S. has been supported by Österreichischen Fonds zur Förderung der wissenschaftlichen Forschung, Project Y123-INF.

References

[1] M. L. Agranovsky, and E. T. Quinto. *Injectivity Sets for the Radon Transform over Circles and Complete Systems of radial Functions.* Journal of Functional Analysis, pp. 383-414. 1996.

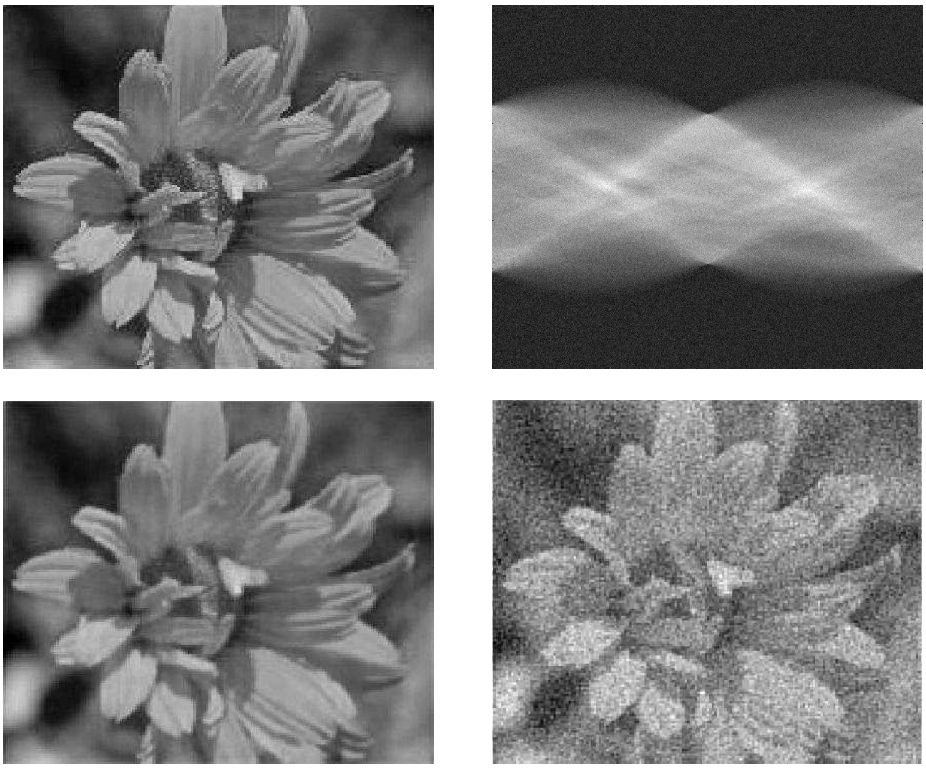

Figure 3: *Top Left:* Synthetic data from which the thermoacoustic pressure signal is calculated numerically. *Top Right:* Random perturbation of $\bar{g}$ with 10% additive Gaussian noise (time versus angle). *Bottom Left:* Reconstruction from exact data. *Bottom Right:* Reconstruction from noisy data.

[2] L.-E. Andersson. *On the determination of a function from spherical averages.* SIAM J. Math. Anal., Vol. 19, pp. 214-232. 1988.

[3] J. A. Fawcett. *Inversion of n-dimensional spherical averages.* SIAM J. Appl. Math. 45, pp. 336-341. 1985.

[4] D. Finch, S. K. Patch, and Rakesh. *Determining a function from its mean values over a family of spheres.* SIAM J. Math. Anal., Vol. 35, pp. 1213-1240. 2004.

[5] S. Helgason. *The Radon transform, Second Edition.* Progress in Mathematics, Birkhäuser, 1999.

[6] V. E. Gusev, A. A. Karabutov *Laser Optoacoustics.* American Institute of physics. New York, 1993.

[7] F. John. *Partial Differential Equations.* Springer-Verlag, 1982.

[8] K. P. Köstli, D. Frauchinger, J. J. Niederhauser, G. Paltauf, H. W. Weber, and M. Frenz. *Optoacoustic imaging using a three-dimensional reconstruction algorithm.* IEEE Journal in Quantum electronics 7(6). 2001.

[9] R. A. Kruger, D. R. Reinecke, G. A. Kruger. *Thermoacoustic computed tomography–technical considerations.* Medical Physics, Volume 26, Issue 9, pp. 1832-1837. 1999.

[10] R. A. Kruger, W. L. Kiser, K. D. Miller, H. E. Reynolds. *Thermoacoustic CT: imaging principles.* Proc SPIE 3916, pp. 150-159. 2000.

[11] R. A. Kruger, K. M. Stantz, and W. L. Kiser. *Thermoacoustic CT of the Breast.* Proc. SPIE 4682, pp. 521-525. 2002.

[12] P. Liu. *Image reconstruction from photoacoustic pressure signals.* Proceedings of the Conference of Laser-Tissue Interaction VII, Proc. SPIE 2681, pp. 285-296. 1996.

[13] F. Natterer. *The mathematics of computerized tomography.* SIAM Classics in Applied Mathematics, 2001.

[14] F. Natterer, and F. Wübbeling. *Mathematical methods in image reconstruction.* Society for Industrial and Applied Mathematics (SIAM), Philadelphia, PA, 2001.

[15] M. Xu, and L.-H. Wang. *Time-domain Reconstruction for Thermoacoustic Tomography in a Spherical Geometry.* IEEE Trans. Med. Imag., 21(7), pp. 814-822. July 2002.

[16] Y. Xu, D. Feng, and L.-H. Wang. *Exact Frequency-domain Reconstruction for Thermoacoustic Tomography–I: Planar Geometry.* IEEE Trans. Med. Imag., 21(7), pp. 823-828. July 2002.

[17] Y. Xu, M. Xu, and L.-H. Wang. *Exact Frequency-domain Reconstruction for Thermoacoustic Tomography–II: Cylindrical Geometry.* IEEE Trans. Med. Imag., 21(7), pp. 829-833. July 2002.

[18] X. Wang, Y. Pang, G. Ku, X. Xie, G. Stoica, and L.-H. Wang. *Noninvasive laser-induced photoacoustic tomography for structural and functional in vivo imaging of the brain.* Nature Biotechnology 21 (7), pp. 803-806. July 2003.

[19] M. Xu and L.-H. Wang. *Analytic explanation of spatial resolution related to bandwidth and detector aperture size in thermoacoustic or photoacoustic reconstruction.* Physical Review E 67(5), pp. 1-15. May 2003.